JCI insight

Sensitive and adaptable pharmacological control of CAR T cells through extracellular receptor dimerization

Wai-Hang Leung, … , Jordan Jarjour, Alexander Astrakhan

JCI Insight. 2019. https://doi.org/10.1172/jci.insight.124430.

Research In-Press Preview Oncology Therapeutics

Graphical abstract

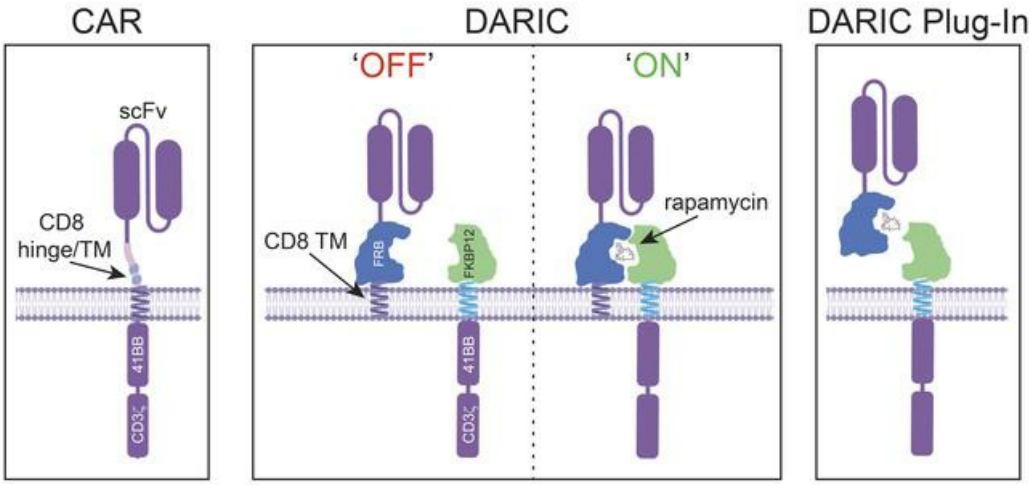

Sensitive and Adaptable Pharmacological Control of CAR T cells Through Extracellular Receptor Dimerization

Wai-Hang Leung[1], Joel Gay[1], Unja Martin[1], Tracy E. Garrett[1], Holly M. Horton[1], Michael T. Certo[1], Bruce R. Blazar[2], Richard A. Morgan[1], Philip D. Gregory[1], Jordan Jarjour[1], Alexander Astrakhan[1]

[1]bluebird bio, inc., Cambridge, MA, USA. [2]Department of Pediatrics, Division of Blood and Marrow Transplantation, University of Minnesota, Minneapolis, MN, USA.

Conflict of interest: All authors, except BRB, are employees and shareholders of bluebird bio. WHL, JG, MTC, JJ and AA are co-inventors on patent applications describing the DARIC technology. BRB declares no conflict of interest.

Abstract

Chimeric antigen receptor (CAR) T cell therapies have achieved promising outcomes in several cancers, however more challenging oncology indications may necessitate advanced antigen receptor designs and functions. Here we describe a bipartite receptor system comprised of separate antigen targeting and signal transduction polypeptides, each containing an extracellular dimerization domain. We demonstrate that T cell activation remains antigen dependent but can only be achieved in the presence of a dimerizing drug, rapamycin. Studies performed *in vitro* and in xenograft mouse models illustrate equivalent to superior anti-tumor potency compared to currently used CAR designs, and at rapamycin concentrations well below immunosuppressive levels. We further show that the extracellular positioning of the dimerization domains enables the administration of recombinant re-targeting modules, potentially extending antigen targeting. Overall, this novel regulatable CAR design has exquisite drug sensitivity, provides robust anti-tumor responses, and is uniquely flexible for multiplex antigen targeting or retargeting, which may further assist the development of safe, potent and durable T cell therapeutics.

Introduction

Therapies that harness the immune system are transforming cancer care. From antibody-mediated programmed cell death protein 1 (PD-1/PD-L1) checkpoint blockade to chimeric antigen receptor (CAR) T cells, these approaches expand antigen specific T cells and can efficiently eliminate antigen positive tumor cells. Unlike checkpoint blockade, CAR T cells target and eliminate target cells directly, enabling treatment of patients lacking HLA-presented neo-epitopes or pre-existing tumor infiltrating lymphocytes(1). Multiple clinical trials are underway to test CAR T cell efficacy in diverse hematologic and solid tumor indications, with the most promising results coming from trials targeting CD19+ or B Cell maturation antigen (BCMA+) cancers(2). Long term remission rates as high as 50% have been reported in patients receiving CAR T therapy and the first two CD19-targeting CAR therapies were granted FDA approval in 2017 for particular B cell cancers(3–6).

Despite encouraging early clinical responses, safety and efficacy remains a challenge for CAR T cell therapies(7). Many CAR T cell responses are associated with antigen-induced cytokine release syndrome (CRS) of varying severity(8). CAR T cells targeting CD19 can also cause severe neurotoxicity, increased risk of infection and chronic B cell aplasia requiring prolonged intravenous immunoglobulin (IVIG) replacement therapy(3, 4, 9, 10). These safety concerns are not constrained to hematopoietic cancers, as clinical trials in other oncology indications have reported excessive and occasionally lethal CAR T cell activity due to antigen expression on normal tissue(7). Following CAR T cell treatment, disease relapses can occur due to antigen escape, T cell exhaustion or CAR-directed immune rejection(11–14). Even with excellent potency, these properties may limit the success of CAR T cell therapies to a small number of indications.

Most clinically relevant features of CAR T cell biology, including expansion, biodistribution, effector and memory formation are regulated, directly or indirectly, through antigen receptor signaling. Most CAR constructs are typically comprised of a single-chain antibody variable domain (scFv) coupled via hinge and transmembrane spanning motifs to intracellular costimulatory and activation domains(1, 8). This design drives continuous T cell activation as long as antigen-positive cells are present. In the case of CD19-directed therapies, patients with high tumor burden experience greater initial CAR T cell expansion and become at risk for developing severe CRS and associated sequelae due to fulminant T cell activation(15). Since tumor cellularity is extremely variable within and across tumor types and indications, CAR T therapies have

disparate pharmacokinetic properties that are difficult to predict and that do not correlate well with the initial dose(15, 16). Further, in contrast with sterilizing immune responses that eliminate antigen, continuous antigen exposure in a setting of chronic infection or cancer is known to drive a progressive loss of T cell effector function, culminating in exhaustion and defective memory formation(17, 18). Similarly, persistent exposure to CD19 antigen drove T cell exhaustion in a syngeneic mouse with constitutively active CD19-CAR T cells(19). The inability to control CAR T cell activation following infusion substantially impacts safety and potentially limits anti-tumor responses. Improved CAR architectures, in particular designs that circumvent constitutive antigen-dependent signaling, may be necessary for CAR T cells to successfully address complex and heterogeneous solid and liquid tumors.

Novel CAR designs that allow for controlled T cell activation have been described and vary from universal epitope-specific small molecule regulated CARs(20–24). In addition, CARs that target tumors using separately infused antibodies are in early stage clinical trials(25). Here, we describe a controllable and adaptable antigen recognition system termed dimerizing agent regulated immune-receptor complex (DARIC). We show that DARIC T cells drive highly potent *in vitro* and *in vivo* anti-tumor responses even at sub-immunosuppressive rapamycin dosing. By providing a 'plug-in' – recombinant subunit containing a separate single chain variable fragment (scFv)-based targeting domain – we show extended targeting and functionality of DARIC T cells to a second antigen. We also demonstrate that DARIC T cells can be reactivated following extended periods of drug cessation. DARIC is thus a highly customizable and potent signaling architecture for next generation T cell therapy applications that is easily toggled between on and off states using rapamycin.

Results

CD19-DARIC component design

We initially developed DARIC constructs targeting the human CD19 antigen for comparison with well characterized CD19 CAR T cells. The CD19-DARIC has a split-receptor design segregating the antigen binding and intracellular signaling subunits into two membrane-tethered polypeptides that dimerize in the presence of rapamycin. The antigen recognition subunit contains an N-terminal CD19 targeting scFv (clone FMC63) fused to the FK506 binding protein (FKPB12) and a CD4 transmembrane domain. The physically separated signaling subunit contains the FKBP-rapamycin binding (FRB*)(26) domain from the human mTOR complex fused to the CD8α transmembrane domain, followed by the cytoplasmic signaling domains of 4-1BB and CD3ζ (Fig 1A)(27, 28). For lentiviral expression, the two components are linked by a porcine teschovirusvirus-1 2A (P2A) peptide and placed under the control of the myeloproliferative sarcoma virus enhancer, negative control region deleted, dl587rev primer-binding site substituted U3 (MNDU3) promoter. In the absence of rapamycin ("OFF" state), CD19-DARIC T cells may bind CD19+ target cells but do not initiate signal transduction due to the disconnect between the antigen binding and intracellular signaling subunits. Addition of rapamycin, or the non-immunosuppressive rapalog AP21967,(26) dimerizes the two subunits to form a signaling-competent immunoreceptor complex ("READY" state). A second generation CD19-CAR construct containing the identical scFv and a 4-1BB-CD3ζ signaling domain was used as a control in all experiments (Fig. 1B).

The CD19-DARIC expression and T cell characterization

The CD19-CAR and CD19-DARIC T cells were characterized prior to tumor co-culture. Antibody-activated peripheral blood mononuclear cells (PBMCs) were left untransduced (UTD) or transduced with lentiviral vectors and expanded over 10 days followed by characterization of the T cell products. Both CD19-CAR and CD19-DARIC T cells had similar *ex vivo* expansion following lentiviral transduction (data not shown). We next determined the cell surface phenotype of the transduced T cells. It has previously been shown that antigen-independent T cell activation (tonic signaling) results in downregulation of CD62L expression(29, 30). Using CD45RA and CD62L expression profile, we observed a similar phenotype for untransduced cells and for CD19-CAR or CD19-DARIC T cells, suggesting that CD19-DARIC expression does not lead to tonic signaling (Figure 1C).

Both CD19-CAR and CD19-DARIC T cells had similar number of viral integrations as determined by vector copy number (VCN) analysis (CD19-CAR VCN 3.7, and CD19-DARIC VCN 3.1; mean of 3 transductions). Interestingly, CD19-DARIC T cells demonstrated significantly reduced binding of fluorescently labeled recombinant CD19 antigen compared to CAR T cells (Fig 1D, MFI values in red). The decreased staining pattern could be due to lower transgene expression, DARIC instability in the absence of dimerizing agent, inefficient scFv export to the plasma membrane, or steric blockade of scFv binding due to the presence of FKBP12. To investigate this, we performed western blot analysis of CD3ζ expression in total lysates which showed similar CD3ζ levels in CD19-CAR and CD19-DARIC T cells (Fig 1E, left panel). We also used a 2A-specific antibody to probe the efficiency of 2A skipping in the DARIC system. In a complete ribosome skipping process, the 2A peptide remains at the C-terminus of the CD3ζ signaling domain, producing a 38kDa polypeptide(31). Incomplete ribosome skipping will result in the formation of a high molecular weight fusion protein detectable with the 2A-specific antibody(31). A single 38kDa band was detected in DARIC cell lysates, confirming an efficient ribosomal skipping process and suggesting that uncleaved DARIC fusions are unlikely to account for reduced antigen staining (Fig 1E, right panel). Previous studies have shown that both FRB* and FKBP12 can be unstable and degraded in the absence of rapamycin(32, 33), however pre-incubation with rapamycin or AP21967 did not change the CD19-His binding pattern (data not shown). Since antigen binding may be sterically hindered by the presence of the FKBP12 domain, we raised rabbit polyclonal antibodies directed against the FRB-Rapamycin-FKBP12-CD19 to determine whether addition of a dimerizing agent can stabilize complex formation. The polyclonal antibodies recognized CD19-scFv and could be used to stain both CD19-CAR and CD19 DARIC T cells. Addition of either AP21967 or rapamycin had minimal impact on CD19-CAR expression (Fig 1F, left panel). However, extended culture of CD19-DARIC T cells in the presence of either AP21967 or rapamycin resulted in increased staining using the polyclonal antibody staining (Fig 1F, right). Combined, these data suggest that differential surface staining of CD19-DARIC is not due to reduced transgene expression but rather due to a combination of protein instability and steric hindrance blocking CD19-His interaction.

Rapamycin drives antigen-dependent CD19-DARIC activation

The CD19+ acute lymphoblastic leukemia (ALL)-derived Nalm-6 cell line was used for *in vitro* and *in vivo* testing of CD19 CAR and CD19-DARIC T cells. Initially, T cells were co-cultured with GFP+ Nalm-6 cells in a 1:1 effector to target (E:T) ratio for 24hrs in the presence of various concentrations of rapamycin or

AP21967 and IFNγ concentration in the supernatant was analyzed using ELISA. CD19-CAR T cells, but not UTD controls, produced IFNγ when co-cultured with Nalm-6 target cells. We detected minimal cytokine secretion when CD19-DARIC T cells were exposed to Nalm-6 cells without dimerizing drug. However, when CD19-DARIC T cells were co-cultured with Nalm6 in the presence of rapamycin or AP21967, we observed equivalent or even greater level of IFNγ secretion compared to CAR controls. Notably, initial rapamycin or AP21967 titration experiments had minimal dose response, with a cytokine production plateau at the lowest dose (Fig 2A-B). We titrated the rapamycin concentration further to determine if CD19-DARIC T cells still respond at low rapamycin dosing. Rapamycin, but not AP21967, reduced CAR-mediated cytokine production in a concentration-dependent manner (Fig 2C). Interestingly, CD19-DARIC T cells were activated at low rapamycin concentrations and produced higher cytokines levels compared to CD19-CAR T cells when cultured with AP21967 or low rapamycin doses (Fig 2C). Neither the CAR nor DARIC T cells showed substantial cytokine production in the absence of target cells, even in the presence of rapamycin (data not shown).

We used a FACS-based cytotoxicity assay to analyze the lytic activity of CAR and DARIC T cells. While CAR T cells eliminated 85% of GFP+ Nalm-6 cells in a 24hr co-culture assay, CD19-DARIC T cells had minimal cytotoxicity (~20%) in the absence of rapamycin or AP21967 (Fig. 2D). Addition of rapamycin (1nM) or AP21967 (20nM), however, produced equivalent level of cytotoxicity of CD19-CAR T cells (~80%, Fig 2D). We also used live cell imaging to analyze the kinetics of tumor cell killing with CD19-CAR or CD19-DARIC samples. The adherent A549 tumor line was stably transduced with CD19 and a red reporter and cultured with CD19-CAR or CD19-DARIC cells in the presence or absence of dimerizing agents. Tumor growth was analyzed by IncuCyte live cell imager. The A549 cells grew normally in the presence of rapamycin or untransduced T cells, while co-culture with CD19-CAR T cells resulted in tumor elimination (Fig S1A). The CD19-DARIC T cells exhibited some antigen-specific cytotoxicity in the absence of rapamycin, however addition of either rapamycin or AP21967 resulted in equivalent cytotoxicity compared to CD19-CAR controls. Notably, the CD19-CAR and CD19-DARIC T cells exhibited similar cytotoxicity kinetics in the presence of dimerizing drug, suggesting that the dimerization process does not delay T cell activation. Similar to data shown in Fig 2A-C, the activity of CD19-CAR T cells was slightly suppressed by rapamycin while CD19-DARIC T cells exhibited equivalent cytotoxicity in the presence of either rapamycin or AP21967. As expected, we saw no cytotoxicity with either CD19-CAR or CD19-

DARIC T cells when cultured with A549 cells transduced with a control BCMA antigen (Fig S1B).

Using incorporation of 5-ethynyl-2'-deoxyuridine (EdU) as a surrogate readout of T cell proliferation, we detected similar proliferation level for both CAR and CD19-DARIC T cells when cultured in the presence of Nalm-6 targets and rapamycin. However, CD19-DARIC T cells had minimal EdU uptake when cultured in the absence of a dimerizing agent (Fig 2E). Combined, these findings demonstrate that the DARIC signaling architecture displayed a minimal basal activity and only gains signaling competency in the presence of a dimerization agent.

Rapamycin drives antigen-dependent elimination of ALL-derived B cell lines

Acute lymphoblastic leukemia is a highly heterogenous disease with different levels of CD19 expression, multiple potential genetic alterations and various ways to block immune recognition of the tumor. We tested the responsiveness of CD19-CAR and CD19-DARIC T cells to various ALL-derived tumor cell lines that expressed different amounts of CD19 antigen (Fig S2A). The CD19-CAR T cells secreted cytokines when co-cultured with all the ALL tumor cell lines. Cytokine production was mostly correlated to CD19 expression, with exception of GM20390, which induced considerably lower levels of cytokine secretion despite expressing intermediate levels of CD19. Notably, the CD19-DARIC T cell did not produce cytokines when cultured with tumor cells alone. However, with the exception of GM20390 cell line, addition of either rapamycin or AP21967 induced considerable cytokine production, with cytokine secretion levels positively correlated to CD19 expression (Fig S2B). As expected, addition of rapamycin was immunosuppressive to CD19-CAR T cells, with reduced cytokine production compared to rapamycin treated CD19-DARIC T cells for nearly all the cell lines (Fig S2B).

The CD19-DARIC T cells are active at low rapamycin dosing and recognize minimal amounts of CD19 antigen

The typical rapamycin clinical dose results in a 3-15nM trough rapamycin concentration(34). To determine if CD19-DARIC T cells would be primed by sub-clinical rapamycin concentrations, CD19-DARIC T cells were co-cultured with Nalm6 cells in the presence of different concentration of rapamycin. Notably, even a very low rapamycin concentration (1pM) induced some antigen-mediated cytokine production from CD19-DARIC T cells (Fig 3A). Cytokine production increased with higher rapamycin concentration, plateauing

at 100pM, suggesting that CD19-DARIC T cells are active at sub-clinical rapamycin concentrations.

The expression of CD19 is a key variable for effective CAR response, and CD19 antigen downregulation can mediate tumor escape and the loss of CD19-CAR activity(11). Surprisingly, *in vitro* experiments showed higher cytokine production from CD19-DARIC T cells compared to CD19-CAR T cells (Fig 2 and S2). To determine if CD19-DARIC T cells were more sensitive to CD19 antigen expression, $CD19^{neg}$ K562 cells were transfected with different amounts of CD19 mRNA. Following 24hrs, the transfected K562 exhibited a concentration-dependent range of CD19 expression (Fig 3B). The K562 cells were co-cultured with CD19-CAR or DARIC T cells for additional 24hrs in the presence of the biologically inert dimerizing agent AP21967 and supernatants were collected for cytokine analysis. The co-culture was continued for 3 additional days to analyze antigen-induced T cell proliferation. At the conclusion of the co-culture (4 days post-activation), the number of T cells in each sample was counted (Fig 3C). There was no CD19-DARIC T cell expansion in the absence of AP21967, even at very high levels of CD19 expression. Conversely, CD19-CAR T cells exhibited antigen dose-dependent T cell growth, with similar proliferation rates in the presence or absence of AP21967. Interestingly, CD19-DARIC T cells had some, albeit minimal cell growth when cultured with AP21967 alone. However, co-culture of CD19-DARIC T cells with both AP21967 and K562-CD19 target cells resulted in antigen-dependent increase in T cell proliferation. There was a significantly higher expansion of CD19-DARIC T cells compared to CD19-CAR T cells, but only at the low CD19 dose levels (Fig 3C), with CD19-CAR and CD19-DARIC expansion plateauing at higher antigen densities. We observed a similar pattern with cytokine production, with generally level of cytokine production from CD19-DARIC T cells at all levels of CD19 expression (Fig 3D) Higher cytokine production was particularly notable at low CD19 expression for all cytokines tested. Combined, these data demonstrated exquisite sensitivity of CD19-DARIC T cells to both rapamycin concentration and antigen expression and suggest that CD19-DARIC T cells are more likely to respond to low antigen expression compared to CD19-CAR T cells.

DARIC plug-in expands antigen recognition diversity of CAR T cells

The extracellular positioning of the FRB domain in the DARIC system means that this domain is potentially available to partner with other extracellular FKBP12-containing antigen binding components. We explored whether a secondary FBKP12-conjugated scFv, termed DARIC plug-in, can broaden the antigen reactivity

of CAR T cells (Fig 4A). We made recombinant plug-in proteins targeting CD19 (Fig 4B) and BCMA (not shown). The plug-in protein was produced in 293T cells and used without further purification or purified using an FKBP12 affinity column. We tested the potential utility of the plug-in in two different DARIC applications.

First, we tested whether the BCMA plug-in is able to provide secondary antigen specificity for CD19-DARIC T cells. The BCMA plug-in is a previously described BCMA-specific scFv(35) conjugated to FKBP12. We cultured CD19-DARIC T cells with BCMA+ K562 cells, either alone or in the presence of rapamycin. As expected, we saw minimal cytokine production with or without rapamycin. Addition of a rapamycin pre-bound BCMA plug-in, however, resulted in antigen-specific cytokine production. This was a dose-dependent finding, as more recombinant BCMA plug-in led to high levels of cytokine secretion (Fig 4C). Next, we reversed this approach and used a BCMA-specific DARIC with a CD19 plug-in. The BCMA-DARIC construct is similar in design to the CD19-DARIC but utilizes a BCMA-specific scFv(35). We took cultures of BCMA-DARIC in the "off-position" without the addition of rapamycin and added the CD19-plug-in that had been pre-bound with rapamycin and cultured these cells with $BCMA^{-}/CD19^{+}$ antigen positive Nalm-6 cells. Analysis of co-culture cell media 24 hours later demonstrated successful re-direction of BCMA-DARIC T cells to target Nalm-6 cells using the CD19 plug-in (Fig 4D & E).

Next we modified a standard BCMA CAR by inserting an FRB* domain between the scFv and CD8α-hinge region (fig 4F). These T cells, termed adaptable-CAR T cells, retain the antigen specificity of parental BCMA CAR T cells as determined with cytotoxicity and cytokine production assays (Fig. 4G&H). To determine if the CD19 plug-in can function in this context, we added rapamycin-bound CD19 plug-in to cultures and set up a Nalm-6 co-culture. As expected, neither BCMA-CAR nor BCMA-adaptable-CAR T cells exhibited functional responses to BCMA-negative Nalm-6 cells. However, addition of recombinant CD19 plug-in (1.25 μg/ml) to BCMA-adaptable-CAR T cells, but not to BCMA-CAR T cells, induced cytotoxic and cytokine responses to CD19+ Nalm6 cells in tumor co-cultures (Fig 4I&J). Combined, these findings demonstrate that DARIC T cells can be redirected to target a different antigen by rapamycin-ready DARIC plug-in molecules.

DARIC T cells exert effective in vivo tumor control induced by rapamycin or AP21967

To evaluate the *in vivo* anti-tumor efficacy of CD19-DARIC T cells, we established a xenograft mouse model using NOD-SCID-IL2Rgc gamma (NSG) mice injected with Nalm-6 stably expressing firefly luciferase (Nalm6-FFluc). A $1x10^6$ dose of Nalm6-FFluc cells was injected intravenously (iv) into NSG mice on day 1, and $1x10^7$ total T cells were injected iv on day 10, after tumor engraftment was confirmed via bioluminescence. Starting on day 9, mice were given daily IP injections of vehicle (DMSO), rapamycin (0.5 or 1 mg/kg) or AP2167 (4 mg/kg). Bioluminescence analysis of tumor grown was performed every 3-4 days (Fig 5A). The CD19-CAR or CD19-DARIC T cells had a similar cellular phenotype prior to injection (Fig 1E).

Similar tumor burden was seen in mice that received Nalm6-FFluc alone, Nalm6-FFluc with rapamycin/ AP21967, or Nalm6-FFluc with untransduced T cells. Conversely, treatment with CD19-CAR T cells led to rapid and sustained decrease in Nalm6 tumor burden (Fig 5B, dark blue). Consistent with the immunosuppressive effect of rapamycin, rapamycin treatment of CD19-CAR T cells slightly reduced Nalm6 tumor control *in vivo* (Fig 5B, light blue).

The *in vivo* activity of CD19-DARIC T cells was completely dependent on rapamycin. In the absence of drug, mice treated with CD19-DARIC T cells had no appreciable decrease in tumor burden (Fig. 5B, purple). However, administration of rapamycin or AP21967 resulted in equivalent level of tumor clearance compared to mice receiving CD19-CAR T cells (Fig 5B, red curve). Notably, the level of tumor control was similar with all the tested doses of rapamycin or AP2167. No immunosuppressive effect of rapamycin was observed with CD19-DARIC T cells (Fig 5B-D), even when comparing mice that received rapamycin or the non-immunosuppressive AP2167 rapalog (Fig 5B vs 5D).

We investigated whether the activity of CD19-DARIC T cells could be modulated by stopping drug treatment. The AP2167 dosing was stopped after 26 days and the animals were monitored for tumor recurrence for additional 30 days. While Nalm6 levels were unchanged in mice treated with CD19-CAR T cells, CD19-DARIC mice had detectable tumor growth less than 7 days after AP21967 was stopped (Fig 5D). These results suggest that the anti-tumor response of DARIC T cells can be regulated using controlled drug dosing.

DARIC T cells control tumors in vivo at low cell numbers

To determine whether CD19-DARIC T cells are able to control tumor growth at limiting T cell numbers, we infused tumor-bearing mice with different amounts of CD19-CAR or CD19-DARIC T cells. We used the Nalm6/NSG tumor mice described in figure 5 for all studies, and a single rapamycin dose (0.2mg/kg, IP, daily) was used for all treated mice. All T cell preps had a similar phenotype and CD4:CD8 ratio (Fig S3A) and were dose on the basis of CAR/DARIC positivity (Fig S3B). As expected, CD19-CAR, but not CD19-DARIC controlled tumor growth in the absence of rapamycin. While we didn't see any tumor control with a $1x10^6$ CAR/DARIC cell dose, we saw equivalent tumor control for both CAR and DARIC T cells at $5x10^6$ and $15x10^6$ T cell doses (Fig S3C). The $5x10^6$ T cell dose exhibited sub-optimal tumor control compared to $15x10^6$ cell dose, however we observed similar clearance kinetics for both dose groups. A single mouse in the 5x106 CD19-DARIC dose group had minimal tumor control, suggesting a potential issue with T cell infusion. However, the rest of the individual animals for the $5x10^6$ dose had very similar levels of tumor controls, suggesting that CD19-CAR and CD19-DARIC exhibit similar level of activity *in vivo* even at low T cell dosing (Fig S3C).

Non-immunosuppressive rapamycin dosing drive highly potent CD19-DARIC activity in vivo

In the transplantation setting, rapamycin is typically administered as part of an immunosuppressive cocktail to reduce graft rejection and dampen the immune response. The rapamycin immunosuppressive window corresponds to a 3-15 ng/ml trough level in whole blood(36, 37). While we observed equivalent CD19-DARIC activity in the initial dose titration study, we wanted to perform additional rapamycin titration to determine whether the CD19-DARIC T cells were able to control tumor growth at non-immunosuppressive rapamycin concentrations. Nalm6-ffluc cells were inoculated into NSG mice and CD19-DARIC or CD19-CAR T cells were injected at day 10 after tumor inoculation. Mice started receiving daily injections of either 0.1 mg/kg or 0.01 mg/kg rapamycin (qd) at 9 days after tumor injection. Alternatively, mice were treated with 0.1 mg/kg rapamycin every other day (qad, Fig 6A). Due to different tumor engraftment kinetics compared to Fig 5, all the mice that received CD19-CAR T cells had detectable Nalm6 luciferase at all time-points, with or without rapamycin treatment (Fig 6B). As seen previously, mice that received CD19-DARIC T cells in the absence of rapamycin had equivalent tumor growth as the control group. Strikingly, the CD19-DARIC T cells exhibited complete tumor control and had superior tumor elimination compared to CD19-CAR groups (Fig 6B, red vs. blue lines). Further, the CD19-DARIC groups exhibited similar tumor control at the tested

rapamycin doses. We used whole blood sampling to determine the *in vivo* rapamycin trough concentration. Whole blood was sampled from all mice 24hr (qd) or 48hr (qad) following the last rapamycin dose and rapamycin concentration was determined by LC-MS/MS. The highest rapamycin dose (0.1 mg/kg, qd) produced a 10.4 ng/ml rapamycin trough level, while both the 0.1 mg/kg QAD and 0.01 mg/kg qd groups had lower trough concentrations (3.96 ng/ml and 0.7 ng/ml respectively), with 2/5 mice in the 0.01 mg/kg group having rapamycin concentration below the limit of detection (<1 ng/ml) (Fig 6C). Combined, these findings demonstrate that CD19-DARIC T cells are highly active at non-immunosuppressive rapamycin dosing and may have superior *in vivo* activity compared to standard CD19-CAR T cells.

Tunable in vivo tumor control using CD19-DARIC with rapamycin pulsing

Previous data (Fig 5) suggested that CD19-DARIC T cells exert continuous tumor control in the presence of a dimerizing agent and the tumor rebounds once drug dosing is stopped. To test whether the rapamycin dose impacts tumor recurrence, drug dosing was stopped 28 days after tumor inoculation and the CD19-DARIC mice were monitored for tumor relapse (Fig 6D). While all drug treated groups had similar level of tumor control in the presence of rapamycin, all animals treated with the lowest rapamycin dose (0.01 mg/kg) had tumor recurrence within 20 days after drug cessation. Higher rapamycin dosing tended to result in longer remissions (Fig 6D, 0.1 vs. 0.01), however there was no significant difference in time to relapse between different rapamycin dosing. All the mice in the 0.01 mg/kg qd and 0.1 mg/kg qad group relapsed, while 4/5 mice in the 0.1 mg/kg qd group relapsed. We monitored each group of mice for tumor recurrence and rapamycin treatment was restarted following a positive luciferase signal (Fig 6D, red lines). While none of the mice in the 0.01 mg/kg qd group achieved tumor control after rapamycin re-dosing, 2/5 animals in the 0.1 mg/kg qad group and 2/4 mice in the 0.1 mg/kg qd group had decreased tumor bioluminescence following rapamycin re-dosing. These observations demonstrate that CD19-DARIC T cells actively suppress tumor growth in the presence of rapamycin and periodic drug re-treatment can re-activate DARIC functionality *in vivo*.

Discussion

Targeting CD19+ B cell cancers with CAR T cells has produced exceptional clinical outcomes, culminating with the approval of two CD19-targeting CAR products within the past year. Consequently, the next generation of CD19 targeting CAR products must produce equivalent or greater efficacy while improving safety and incorporating multiplex antigen targeting capacity. The findings presented in this study show that the drug regulatable DARIC system exhibits similar or greater efficacy in eliminating tumor cells *in vitro* and *in vivo* compared to currently used CAR T cell designs. Tumor elimination is fully drug-dependent and tumor control is lost once drug dosing is stooped. In addition, we show that the extracellular positioning of the FKBP12 domain enables DARIC T cells retargeting towards additional antigens. Combined, our results establish the DARIC system as a flexible and powerful antigen targeting platform to create better T cell therapies.

Several other regulatable CAR approaches have been described, including variants that have dimerizable subunits and systems using universal adapter CARs(22, 24, 32, 38). Lim and colleagues designed a system which also uses the FKBP12 and FRB components to regulate CAR activity(22). Unlike DARIC, their approach placed the dimerization domains intracellularly to regulate CAR activity. Intracellular localization of FKBP12 and FRB could hinder or alter signal transduction events and could be susceptible to competition with endogenous FKBP12 and mTOR binding proteins. Consequently, this system required considerably higher dimerizing agent concentrations for activity and did not achieve parity with a CD19 CAR control in vitro or in vivo(22). In addition, Juillerat and coworkers published a rapamycin-regulated system with extracellular positioning of the FRB/FKBP12 dimerizing domains, similar to the DARIC system (32). Similar to data shown in Figure 1F, the authors showed that rapamycin stabilized expression of an FRB/FKBP12 signaling architecture, while addition of FK506 blocked the dimerization and led to reduced expression. However, they used an FcεRI-based signaling and dimerization architecture and had minimal *in vitro* and no *in vivo* functional validation, making it difficult to compare their approach to the DARIC system. Further, the compatibility and efficiency of the DARIC system with the use of rapamycin, a very well characterized clinical agent, could potentially streamline the translation of the DARIC system to the clinic.

The DARIC plug-in approach expands the potential utility of the DARIC system. We describe two different ways to utilize the plug-in approach to retarget T cells towards a second antigen. Notably, both the adaptable CAR and the DARIC approach are compatible with rapamycin pre-loaded plug-in proteins. Using rapamycin preloading simplifies clinical use, as rapamycin pre-bound plug-in scFvs do not need additional rapamycin to bind the target T cells. Due to the high affinity between FKBP12 and rapamycin (0.2nM)(39), rapamycin pre-bound scFv should not disassociate from rapamycin *in vivo*, lessening the risk of inadvertent immunosuppression. The kinetics of FKPB12-rapamycin disassociation depend on the availability of DARIC T cells, which will serve as binding and stabilizing partner for the FKBP12-scFv domain. Notably, several adapter-based CAR architectures have been described(21, 24, 40, 41), using a combination of epitope or linker based universal CARs. The DARIC architecture combines the antigen flexibility of the universal CAR approach with the functionality and efficacy of traditional single antigen CAR T cell. This allows stepwise development of the DARIC system, starting with a validated CAR target and progressing to secondary antigen targeting once the initial DARIC approach has been clinically tested. As shown in Figures 5-6, CD19-DARIC T cells had similar steady state anti-tumor activity at all rapamycin doses tested, and we did not determine the minimal rapamycin dose for complete *in vivo* response. Partly, this reflects the exquisite sensitivity of the DARIC system even at low rapamycin levels, likely due to the extracellular placement of the dimerization machinery. However, due to this sensitivity, it is difficult to determine the on/off kinetics of the DARIC system *in vivo*. The CD19-DARIC treated mice exhibited similar speed and depth of tumor control at all rapamycin doses (Figures 5-6). Further, all the treated mice exhibited tumor relapse after cessation of treatment. While the kinetics of relapse may have been faster in animals treated with lowest dose of rapamycin, these differences were not statistically significant (Figure 6D). Notably, the animals that were able to control the tumor relapse did so rapidly after rapamycin re-initiation, suggesting that the CD19-DARIC system can rapidly turn on after provision of the dimerizing agent. Future experiments using T cell, rapamycin and FK506 dose titrations will determine the full on/off kinetics of the CD19-DARIC system in steady state tumor growth versus relapse.

Rapamycin has wide applications in both transplantation and oncology(37, 42). It is available in oral and intravenous formulations and has clearly defined pharmacokinetic and pharmacodynamic properties in both adult and pediatric populations. Since rapamycin has a considerably shorter half-life in mice (~15 hours)(43) compared to adult humans (~60 hours)(42), interpolating clinical dosing from mouse studies is complicated.

However, the high activity of CD19-DARIC T cells at all tested doses potentially enables considerable clinical dosing flexibility. Weekly sub-immunosuppressive oral rapamycin, higher dose immunosuppressive regimens to promote competitive DARIC T cell engraftment, episodic dosing to mitigate T cell exhaustion, or the use of alternative rapamycin formulations, such as everolimus or temsirolimus are all potentially available as interventions to fine tune T cell activation dynamics.

By inhibiting mTOR signaling, rapamycin is broadly immunosuppressive at medium and high doses, impacting all stages of the immune response, including T and B cell activation, antigen presentation and natural killer responses(44). At the same time, rapamycin treatment has also been shown to enhance $CD8^+$ T cell memory formation by promoting the lipid metabolism pathway at the expense of the glycolytic metabolism used by CD8 effector cells(45, 46). Notably, rapamycin-mediated T cell memory formation is highly dependent on the dose and timing of rapamycin in the context of a broader immune response(46). Improved responses to immunization and reduced infection rates in elderly patients treated with low dose everolimus alone or in combination with a catalytic mTOR/PI3K inhibitor have been reported in a clinical trial setting(47). Given these observations and the low rapamycin dose requirements established in our DARIC studies, the rapamycin treatment component of putative DARIC T cell therapies should either have a minimal systemic effect, or may even slightly dampen the broader immune response, modulating the intensity and onset of treatment-related CRS and/or the development of the bystander T cell response.
The formation of a functional T cell memory pool depends on multiple factors, including expression of appropriate costimulatory ligands, favorable nutrient availability, concentrations of cytokines, and, most importantly, the magnitude and duration of antigen-specific T cell response. Persistent and chronic T cell activation may induce T cell exhaustion instead of memory formation(17, 48). While multiple factors contribute to the failure of CAR T therapies, these cells often exhibit exhaustion characteristics, such as altered metabolism and upregulation of checkpoint markers, in both clinical and preclinical models. Conceptually, persistent antigen exposure within the solid tumor or through continuous generation of CD19+ target cells may result in the development of T cell tolerance or T cell exhaustion due to chronic CAR stimulation(16, 49, 50). Consistent with this idea, chronic antigen exposure resulted in reduced CD19-CAR T cell persistence in a syngeneic mouse model. Incorporating a rest period between antigen exposure, however, led to drastically enhanced CAR expansion in vivo and a reduced CAR exhaustion profile(19). These and other observations suggest that DARIC activation using pulsatile rapamycin dosing may more

accurately mimic the endogenous immune response and lead to improved T cell memory formation and reduced risk of exhaustion.

The development of regulatable CAR architectures and safety switches has been partially driven by the severe adverse events (SAEs) occasionally seen in CD19 CAR T cell clinical trials. These SAEs present as either rapid onset acute manifestation of cytokine release syndrome (CRS) or more persistent and longer-term neurologic toxicity(9). Other less severe complications from CD19 CAR T cell therapy such as chronic B cell aplasia(3) and increased risk for infections(10) can be divided into short and long-term effects. Acute CRS-related toxicity typically resolves via infusion of αIL-6 antibody (tocilizumab), while neurologic complications take longer to resolve and may have a different underlying mechanism compared to acute CRS(9). Given the sensitivity of the CD19-DARIC system, treatment interruption is not likely to prevent or stop fulminant CRS manifestations. However, a low dose rapamycin treatment combined with neurotoxicity monitoring should enable rapid dose de-escalation once neurological toxicity is observed, potentially reducing or stopping CAR-mediated neurologic SAEs. As a separate safety mechanism, the FKBP12 component of the DARIC system binds FK506 (tacrolimus) in addition to rapamycin(51). In case of severe CRS or persistent neurotoxicity, FK506 administration should reduce rapamycin binding to FKBP12 through competitive inhibition, lessening DARIC activity while inducing general immunosuppression to further dampen a CRS response(36). We are currently investigating whether FK506 administration is able to modulate CD19-DARIC activity *in vitro* or *in vivo*.

In conclusion, the data presented in this manuscript demonstrate the potential of CD19-DARIC T cells for regulated and effective tumor targeting. Unlike other regulatable or apoptosis-based safety systems, the CD19-DARIC approach is just as potent as standard CD19-CAR T cells and can be regulated with clinically relevant rapamycin dosing. These findings support continued development of DARIC T cells for hematopoietic and solid tumor indications.

Materials and Methods

Reagents, antibodies and cell lines

Rapamycin was purchased from Sigma, MO. The non-immunosuppressive rapamycin analog (rapalog) AP21967 was from TaKaRa, CA. Both AP21967 and rapamycin were resuspended in DMSO and diluted in PBS immediately prior to *in vitro* or *in vivo* use. CD19-CAR or CD19-DARIC expression in T cells was detected either by flow cytometry using CD19-HIS PE (Creative Biomart, NY) or by Western blot analysis using rabbit anti-2A polyclonal antibodies (Millipore, MA) and mouse anti-human CD3ζ monoclonal antibody (Santa Cruz, TX). *In vitro* T cell subset development was analysis by flow cytometry with αCD62L-APC (clone DREG-56) and αCD45RA-PECy7 (clone HI100) both from Biolegend (San Diego, CA). 293T cells, Nalm-6 cells and K562 cells were purchased from ATCC, VA. DMEM, RPMI-1640, HEPES, GlutaMax and fetal bovine system (FBS) were purchased from Thermo Fisher, MA. X-VIVO 15 media were purchased from Lonza, NJ. Human AB sera were from Valley Biomedical, WA. 293T cells were cultured in DMEM supplemented with 10 mM HEPES, 2 mM GlutaMax and 10% FBS. Nalm-6 and K562 cells were cultured in RPMI-1640 supplemented with 10 mM HEPES, 2 mM GlutaMax and 10% FBS. T cell growth medium (TCGM) were prepared with X-VIVO 15 supplemented with 10 mM HEPES, 2 mM GlutaMax and 5% human AB serum.

Lentivirus production

Lentiviral production was performed as previously described(35). Briefly, CD19-CAR(52), CD19-DARIC, BCMA-CAR(35), BCMA-DARIC and BCMA-adaptable CAR lentiviral constructs were co-transfected with a three-packaging-vector system into 293T cells using PEI pro reagent (Polyplus, NY). Lentivirus containing culture supernatants were collected, filtered, aliquoted and stored at -80°C 48 h post-transfection. Vector copy number analysis was performed as previously described(35).

Human peripheral blood mononuclear cell (PBMC) culture and lentiviral transduction

Cryopreserved PBMC from healthy donors (Key Biologics, TN) were thawed and cultured in TCGM supplemented with 250 U/ml recombinant human IL-2 (CellGenix, Germany) and 50 ng/ml αCD3 (clone OKT3) and αCD28 (15E8) antibodies (Miltenyi Biotec, CA) on day 0, as previously described(35). Lentiviral supernatant was added to PBMC cultures 24hrs after activation. At 72hrs after activation,

transduced PBMC were collected, washed and resuspended in complete TCGM with human IL-2 at $0.5x10^6$ cells/ml. PBMC cultures were maintained at 0.5 X 10^6 cells/ml with the additional of fresh media every 2 days. Flow cytometry acquisition was performed using an Attune NxT (Thermo Fisher) and the data analyzed using FlowJo (Ashland, OR). *In vitro* functional assays were performed on day 9 and day 10 as described in figure legends.

Western blot analysis

For protein analysis, $2x10^6$ T cells were lysed and prepared in NuPAGE LDS sample buffer (Thermo Fisher, MA), separated with NuPAGE 4–12% Bis-Tris gels, and then transferred onto nitrocellulose membranes using the iBlot transfer system (Thermo Fisher, MA). After incubation with 5% nonfat milk in TBST (10 mM Tris, pH 8.0, 150 mM NaCl, 0.5% Tween 20) for 15 min, the membranes were incubated with antibodies against 2A peptide (rabbit polyclonal, 1:1000 (Millipore, cat #ABS31)), or anti-CD3ζ (mouse monoclonal, 1:1000 (Santa Cruz, clone 6B10.2)) at 4 °C for 16hrs. Membranes were washed three times for 15 min and incubated with a 1:10000 dilution of HRP-conjugated anti-mouse IgG or anti-rabbit IgG (Thermo Fisher, MA) for 1hr. The membranes were washed with TBST five times and developed with the SuperSignal West Femto ECL reagents (Thermo Fisher, MA).

Flow Cytometry cytotoxicity assay

Cytotoxic potential of CD19-CAR and CD19-DARIC T cells was analyzed by co-incubating T cells with 50:50 (%) mixtures of K562.BFP ($CD19^{neg}$) and Nalm-6.GFP ($CD19^{+}$) target cells (with or without 1 nM rapamycin or 20 nM AP21967) for 24 h in an effector to target (Nalm-6) ratio (E:T) at 1:1. The relative percentage of Nalm-6.GFP following T cell co-culture was used to calculated the % specific T cell cytotoxicity:

$$\% \text{ specific cytotoxicity} = ({}_{\% \text{ Nalm-6.GFP}}\text{UTD} - {}_{\% \text{ Nalm-6.GFP}}\text{CD19-CAR or -DARIC}) / {}_{\% \text{ Nalm-6.GFP}}\text{UTD} \times 100\%$$

All analysis was performed on Attune NxT and the data analyzed using FlowJo and GraphPad Prism (San Diego, CA).

Incucyte cytotoxicity assay

For live cell imaging, $5x10^3$ CD19-CAR or CD19-DARIC T cells were co-cultured with $1x10^4$ A549-

NucRed-CD19 cells or A549-NucGreen-BCMA control cells (E:T ratio at 1:2) with or without rapamycin (1 nM) or AP21967 (20 nM) in the IncuCyte S3 (Essen Bioscience, MI) for 4 – 6 days. The live target cells are counted via red or green object counts at indicated time points and data analyzed using the IncuCyte software and GraphPad Prism.

Click-iT EdU T cell proliferation

For proliferative analysis, CD19-CAR or CD19-DARIC T cells T cells ($0.2x10^6$ cells) were co-cultured with Nalm-6.GFP cells for 3 days (E:T ratio at 1:1) with or without rapamycin (1 nM) or AP21967 (20 nM) in 200µl TCGM without IL-2. T cell proliferation was evaluated by using the Click-iT Plus EdU Alexa Fluor 594 flow cytometry assay kit (Thermo Fisher, MA) according to the manufacturer's instruction. Briefly, EdU (4 µM final concentration) was added to the culture for 16 h. Cells were harvested and stained with anti-human CD3 Alex Fluor 647 (Biolegend, CA). T cells were fixed with 40 µl fixative buffer (component D) for 15 min. Washed T cells were then permeabilized in 25 µl 1X Click-iT saponin-based permeabilization and wash reagent for 10 min at room temperature. 125 µl Click-iT reaction mix (prepared according to the manufacturer's manual) was added to each sample and incubated in dark for 30 min. Cells were washed and resuspended in 120 µl permeabilization and wash reagent. EdU incorporation in T cells was analyzed by flow cytometry.

Cytokine production analysis

For cytokine secretion analysis, $0.5x10^6$ T cells were co-cultured with Nalm-6.GFP cells (E:T ratio at 1:1) for 24 h with or without rapamycin (1 nM) or AP21967 (20 nM). Culture supernatants were collected for cytokine (IFNγ and TNFα) detection using the Qbeads PlexScreen kit and analyzed by the iQue Screener (intellicyt, NM).

DARIC plug-in protein production

A CD19-DARIC plug-in producing 293T cell line was generated by transducing 293T cells with a lentiviral vector encoding a human CD19-specific scFv fused to FKPB12 followed by a T2A-mCherry reporter transgene. The transduced cells were sorted for mCherry expression using a FACSAriaII cell sorter (BD Biosciences, CA). To purify recombinant CD19-DARIC plug-in, 500 ml 293T cell culture supernatants were collected and filtered (0.22µm). An FKBP12-specific affinity column was generated by incubating

2 ml NeutrAvidin Agarose (Thermo Fisher, MA) with 400 µg biotin-FK506(53) (LifeTein, NJ) for 30 min at room temperature with constant rotation. The column was washed with PBS to remove uncoupled biotin-FK506. Filtered 293T supernatants were applied to the column by gravity. The column was washed with PBS until A280 of the flow through was 0. CD19-DARIC Plug-in molecules were eluted with 5 ml of 8 µM rapamycin followed by 15 ml PBS. Eluted proteins were concentrated VivaSpin-20 centrifugal concentrator (10kD MWCO) (Millipore, MA) and desalted with Zeba Spin 7K column (Thermo Fisher, MA) to PBS to remove residual unbound rapamycin. The purified protein solution was filtered (0.22µm) sterilized and stored at 4°C. Because of the high affinity between rapamycin and FKBP12 (Kd = 0.2 nM), the purified CD19-DARIC plug-in is stably bound to rapamycin (Rapa-ready CD19 DARIC plug-in). SDS PAGE and Western blot analysis using rabbit anti-FKBP12 antibodies confirmed that the purified protein fraction contained a major protein product with molecular weight of about 40 kDa without detectable lower molecular weight degradation fragments.

Recombinant protein production for rabbit immunization

The CD19 DARIC extracellular domain (FMC63scFv-FKBP12) and FRB were codon optimized for human expression (Integrated DNA Technologies, IA) and cloned by Gibson assembly onto the n-terminus of rabbit IgG or human IgG1 Fc CH2-CH3 respectively (pfuse-rIgG-Fc, pINFUSE, Invivogen, CA). Clones were validated by Sanger sequencing and transfection grade-endotoxin free plasmid was prepared and 0.2um filter sterilized in endotoxin free TE buffer (Qiagen, MD). Protein production was done by transient transfection of Expi293 (Thermo Fisher) cells using manufacturer's recommendation. Briefly, on the day of transfection, cells were seeded at ~2.5e6/ml >95% viability in fresh Expi293 media and grown for ~4-6 hours. Plasmid DNA was diluted to 1ug/ml final volume in OptiMEM-I and PEI (40K, 1mg/ml, Polyplus) was diluted at a ratio of 1:2.5 (DNA:PEI) in OptiMEM-I. After 5-minute incubation, diluted DNA and PEI were combined and incubated for an additional 10-15 minutes before adding drop-wise to cells. Transfected cultures were maintained in 1.6L Thomson shake flasks at 800ml final volume for 5-7 days at 37°C, 8% CO_2, 150 rpm.

For protein purification, cells and debris were pelleted by centrifugation and supernatant was diluted in binding buffer to final concentration 20mM sodium phosphate, pH-7.2, 150mM NaCl followed by 0.2um filtration. Fc tagged proteins were affinity purified on the Akta Explorer-100 FPLC using 5ml HiTrap Protein-A columns (GE Life Sciences), eluted in 0.1M L-Arg-HCl (pH-3.5), immediately neutralized with

1M Tris-Cl (pH-8), concentrated to >1mg/ml (Vivaspin-20 30 or 50kD MWCO) and buffer exchanged to 5% Glycerol/PBS (pH-7.4). Monomeric Fc-tagged proteins were further enriched from higher order aggregate by preparative SEC using a HiLoad 16/600 Superdex 200 pg column (GE Life Sciences). The desired fractions were pooled, concentrated to 1mg/ml, 0.2um filter sterilized and analyzed for purity by SDS-Page.

Polyclonal antibody generation

In order to recapitulate recombinant CD19-DARIC complex antigen, equimolar FMC63scFv-FKBP12-rbFc and FRB-rbFc were prepared in sterile 5% Glycerol/PBS (pH-7.4) to a final concentration of 1mg/ml total protein supplemented with 5umol rapamycin. Injection material was transferred to R&R Research, LLC (WA) and rabbits were immunized according to standard operating protocols.

Rabbit serum was screened for reactivity against the DARIC complex and the individual components by indirect ELISA. Human IgG1-Fc tagged CD19-DARIC, FKBP12 and FRB were coated at 100ng/well in 96-well high protein binding plates (Corning) and incubated overnight at 4°C. Plates were briefly washed in PBS/Tween (PBST) and blocked with 300ul/well 1X ELISA/ELISPOT diluent (Thermo Fisher) for 1-2 hours. A 12-point 2.5-fold serial dilutions of serum pre or test bleed were performed in 1X diluent and 100ul was dispensed per well and incubated for 1 hour. After a brief wash in PBST wells were incubated with a 1:10,000 dilution of Goat-α-Rabbit HRP (Jackson ImmunoResearch, PA) in 1X diluent for 30 minutes. Plates were again washed with PBST and 100ul/well 1-Step Ultra TMB (Thermo Fisher) was added. After development, reaction was stopped with 100ul/well 1N H2SO4 and absorbance at 450nm was measured on a SpectraMax plate reader (Molecular Devices, CA).

Generation of K562 cells expressing various level of CD19 using mRNA electroporation

The CD19 antigen was PCR amplified from a synthetic gBlock (IDT) using CD19-T7 FP (GGATCCTAATACGACTCACTATAGGGGCCGCCACCATGCCACCTCCTCGCCTCCTCTT) and CD19-RP (CTATTAGCGAGTGCTCCAGGTGCCCATGCGGCCC). PCR product was purified with the QIAquick PCR purification kit (Qiagen), the mRNA was synthesized and polyadenylated with the HiScribe T7 ARCA mRNA *in vitro* transcription kit (New England Biolabs, MA) and the mRNA purified with the RNeasy mRNA purification kit (Qiagen) following manufacturer's instructions. The K562 cells were electroporated with indicated amounts of CD19 mRNA using the Neon electroporation system (Thermo

Fisher), using previously described electroporation parameters(54). The electroporated cells were cultured overnight in standard tissue culture conditions and CD19 expression was analyzed by flow cytometry. The cells were counted and used in an AP21967 cytokine co-culture assay as described above.

In vivo mouse xenograft studies

Female 6-10 week old NOD.Cg-*Prkdc*^{scid}IL2rg^{tm1Wjl}/SzJ (NSG) purchased from Jackson Laboratories, Bar Harbor, ME were maintained in the bluebird bio vivarium. All studies were conducted according to a study protocol approved by the bluebird bio Institutional Animal Care and Use Committee. Nalm-6 cell stably expressing firefly luciferase (Nalm-6 FFluc) were used to establish the xenograft model. In all studies, the activity of the CD19-CAR or CD19-DARIC T cells were evaluated by determining the tumor size twice weekly using the IVIS® Spectrum *in vivo* imaging system. General safety was evaluated by observing the animals daily and recording their body weights twice weekly. All in-life personnel were blinded to the identity of the test and control articles. Detailed *in vivo* experiment setup is described in the Results section.

Statistics

Data analysis was performed using GraphPad Prism 7.0, with significance levels described in specific figure legends. A two-tailed unpaired Student's *t*-test was used for statistical comparison of 2 individual groups. A one way ANOVA analysis with Dunnett's test was used for multi-parameter statistical comparisons.

Study Approval

Mouse experiments were performed in Cambridge, MA and approved by the bluebird bio IACUC. All mice were monitored for survival, weight loss and excessive tumor burden, and euthanized according to the IACUC guidelines. All human PBMC lots were purchased from Key Biologics (TN) and obtained under an IRB-approved protocol.

Author contribution

AA, JJ, MC and WHL conceived and designed the DARIC system. WHL, JG, DX and UM conducted the *in vitro* experiments while TV and HMH performed the *in vivo* experiments. BRB, RAM and PDG helped with study design, analysis and manuscript editing. WHL, JJ and AA wrote the manuscript.

Acknowledgements

This study was funded and supported by bluebird bio. The authors want to acknowledge Tejeet Banwait and Seema Shah for help with *in vivo* work, Dong Xia for help with InCyte experiments and Iva Ivanovska Holder for editing contributions and all the members of the bluebird bio Horizon and Immunotherapy groups for helpful discussions.

References

1. Gross G, Eshhar Z. Therapeutic Potential of T Cell Chimeric Antigen Receptors (CARs) in Cancer Treatment: Counteracting Off-Tumor Toxicities for Safe CAR T Cell Therapy. *Annu. Rev. Pharmacol. Toxicol.* 2016;56:59–83.

2. June CH, O'Connor RS, Kawalekar OU, Ghassemi S, Milone MC. CAR T cell immunotherapy for human cancer. *Science* 2018;359(6382):1361–1365.

3. Maude SL et al. Tisagenlecleucel in Children and Young Adults with B-Cell Lymphoblastic Leukemia. *N. Engl. J. Med.* 2018;378(5):439–448.

4. Schuster SJ et al. Chimeric Antigen Receptor T Cells in Refractory B-Cell Lymphomas. *N. Engl. J. Med.* 2017;377(26):2545–2554.

5. Park JH et al. Long-Term Follow-up of CD19 CAR Therapy in Acute Lymphoblastic Leukemia. *N. Engl. J. Med.* 2018;378(5):449–459.

6. Neelapu SS et al. Axicabtagene Ciloleucel CAR T-Cell Therapy in Refractory Large B-Cell Lymphoma. *N. Engl. J. Med.* 2017;377(26):2531–2544.

7. Mirzaei HR, Rodriguez A, Shepphird J, Brown CE, Badie B. Chimeric Antigen Receptors T Cell Therapy in Solid Tumor: Challenges and Clinical Applications [Internet]. *Front. Immunol.* 2017;8. doi:10.3389/fimmu.2017.01850

8. Srivastava S, Riddell SR. Chimeric Antigen Receptor T Cell Therapy: Challenges to Bench-to-Bedside Efficacy. *J. Immunol. Baltim. Md 1950* 2018;200(2):459–468.

9. Gust J et al. Endothelial Activation and Blood-Brain Barrier Disruption in Neurotoxicity after Adoptive Immunotherapy with CD19 CAR-T Cells. *Cancer Discov.* 2017;7(12):1404–1419.

10. Hill JA et al. Infectious complications of CD19-targeted chimeric antigen receptor-modified T-cell immunotherapy. *Blood* 2018;131(1):121–130.

11. Shalabi H et al. Sequential loss of tumor surface antigens following chimeric antigen receptor T-cell

therapies in diffuse large B-cell lymphoma. *Haematologica* [published online ahead of print: February 1, 2018]; doi:10.3324/haematol.2017.183459

12. Gardner R et al. Acquisition of a CD19-negative myeloid phenotype allows immune escape of MLL-rearranged B-ALL from CD19 CAR-T-cell therapy. *Blood* 2016;127(20):2406–2410.

13. Ruella M, Maus MV. Catch me if you can: Leukemia Escape after CD19-Directed T Cell Immunotherapies. *Comput. Struct. Biotechnol. J.* 2016;14:357–362.

14. Jacoby E et al. CD19 CAR immune pressure induces B-precursor acute lymphoblastic leukaemia lineage switch exposing inherent leukaemic plasticity. *Nat. Commun.* 2016;7:12320.

15. Mueller KT et al. Cellular kinetics of CTL019 in relapsed/refractory B-cell acute lymphoblastic leukemia and chronic lymphocytic leukemia. *Blood* 2017;130(21):2317–2325.

16. Fraietta JA et al. Determinants of response and resistance to CD19 chimeric antigen receptor (CAR) T cell therapy of chronic lymphocytic leukemia. *Nat. Med.* 2018;24(5):563–571.

17. Hashimoto M et al. CD8 T Cell Exhaustion in Chronic Infection and Cancer: Opportunities for Interventions. *Annu. Rev. Med.* 2018;69(1):301–318.

18. Wieland D et al. TCF1^{+} hepatitis C virus-specific CD8^{+} T cells are maintained after cessation of chronic antigen stimulation. *Nat. Commun.* 2017;8:15050.

19. Viaud S et al. Switchable control over in vivo CAR T expansion, B cell depletion, and induction of memory. *Proc. Natl. Acad. Sci.* 2018;115(46):E10898–E10906.

20. Bachmann D et al. Retargeting of UniCAR T cells with anin vivosynthesized target module directed against CD19 positive tumor cells. *Oncotarget* 2018;9(7):7487–7500.

21. Ma JSY et al. Versatile strategy for controlling the specificity and activity of engineered T cells. *Proc. Natl. Acad. Sci. U. S. A.* 2016;113(4):E450-458.

22. Wu C-Y, Roybal KT, Puchner EM, Onuffer J, Lim WA. Remote control of therapeutic T cells through a small molecule-gated chimeric receptor. *Science* 2015;350(6258):aab4077.

23. Urbanska K et al. A universal strategy for adoptive immunotherapy of cancer through use of a novel T cell antigen receptor. *Cancer Res.* 2012;72(7):1844–1852.

24. Cho JH, Collins JJ, Wong WW. Universal Chimeric Antigen Receptors for Multiplexed and Logical Control of T Cell Responses. *Cell* 2018;173(6):1426-1438.e11.

25. Motz G et al. Abstract B105: ACTR707: a novel T-cell therapy for the treatment of relapsed or refractory CD20+ B cell lymphoma in combination with rituximab. *Mol. Cancer Ther.* 2018;17(1 Supplement):B105–B105.

26. Bayle JH et al. Rapamycin analogs with differential binding specificity permit orthogonal control of protein activity. *Chem. Biol.* 2006;13(1):99–107.

27. Choi J, Chen J, Schreiber SL, Clardy J. Structure of the FKBP12-rapamycin complex interacting with the binding domain of human FRAP. *Science* 1996;273(5272):239–242.

28. Liberles SD, Diver ST, Austin DJ, Schreiber SL. Inducible gene expression and protein translocation using nontoxic ligands identified by a mammalian three-hybrid screen. *Proc. Natl. Acad. Sci. U. S. A.* 1997;94(15):7825–7830.

29. Long AH et al. 4-1BB costimulation ameliorates T cell exhaustion induced by tonic signaling of chimeric antigen receptors. *Nat. Med.* 2015;21(6):581–590.

30. Kawalekar OU et al. Distinct Signaling of Coreceptors Regulates Specific Metabolism Pathways and Impacts Memory Development in CAR T Cells. *Immunity* 2016;44(2):380–390.

31. Kim JH et al. High Cleavage Efficiency of a 2A Peptide Derived from Porcine Teschovirus-1 in Human Cell Lines, Zebrafish and Mice. *PLOS ONE* 2011;6(4):e18556.

32. Juillerat A et al. Design of chimeric antigen receptors with integrated controllable transient functions. *Sci. Rep.* 2016;6:18950.

33. Edwards SR, Wandless TJ. The Rapamycin-Binding Domain of the Protein Kinase mTOR is a Destabilizing Domain. *J. Biol. Chem.* 2007;282(18):13395–13401.

34. Bäckman L et al. Sirolimus steady-state trough concentrations are not affected by bolus methylprednisolone therapy in renal allograft recipients. *Br. J. Clin. Pharmacol.* 2002;54(1):65–68.

35. Friedman KM et al. Effective Targeting of Multiple B-Cell Maturation Antigen-Expressing Hematological Malignances by Anti-B-Cell Maturation Antigen Chimeric Antigen Receptor T Cells. *Hum. Gene Ther.* 2018;29(5):585–601.

36. Yatscoff RW, Wang P, Chan K, Hicks D, Zimmerman J. Rapamycin: distribution, pharmacokinetics, and therapeutic range investigations.. *Ther. Drug Monit.* 1995;17(6):666–671.

37. Saunders RN, Metcalfe MS, Nicholson ML. Rapamycin in transplantation: A review of the evidence. *Kidney Int.* 2001;59(1):3–16.

38. Foster AE et al. Regulated Expansion and Survival of Chimeric Antigen Receptor-Modified T Cells Using Small Molecule-Dependent Inducible MyD88/CD40. *Mol. Ther. J. Am. Soc. Gene Ther.* 2017;25(9):2176–2188.

39. Banaszynski LA, Liu CW, Wandless TJ. Characterization of the FKBP·Rapamycin·FRB Ternary Complex. *J. Am. Chem. Soc.* 2005;127(13):4715–4721.

40. Rodgers DT et al. Switch-mediated activation and retargeting of CAR-T cells for B-cell malignancies. *Proc. Natl. Acad. Sci.* 2016;113(4):E459–E468.

41. Lee YG et al. Use of a single CAR T cell and several bispecific adapters facilitates eradication of multiple antigenically different solid tumors. *Cancer Res.* 2018;canres.1834.2018.

42. Law BK. Rapamycin: an anti-cancer immunosuppressant?. *Crit. Rev. Oncol. Hematol.* 2005;56(1):47–60.

43. Arriola Apelo SI et al. Alternative rapamycin treatment regimens mitigate the impact of rapamycin on glucose homeostasis and the immune system. *Aging Cell* 2016;15(1):28–38.

44. Thomson AW, Turnquist HR, Raimondi G. Immunoregulatory functions of mTOR inhibition. *Nat. Rev. Immunol.* 2009;9(5):324–337.

45. Pollizzi KN, Powell JD. Regulation of T cells by mTOR: The known knowns and the known unknowns. *Trends Immunol.* 2015;36(1):13.

46. Ferrer IR, Araki K, Ford ML. Paradoxical Aspects of Rapamycin Immunobiology in Transplantation. *Am. J. Transplant. Off. J. Am. Soc. Transplant. Am. Soc. Transpl. Surg.* 2011;11(4):654.

47. Mannick JB et al. TORC1 inhibition enhances immune function and reduces infections in the elderly. *Sci. Transl. Med.* 2018;10(449):eaaq1564.

48. Wherry EJ, Kurachi M. Molecular and cellular insights into T cell exhaustion. *Nat. Rev. Immunol.* 2015;15(8):486–499.

49. Youngblood B et al. Effector CD8 T cells dedifferentiate into long-lived memory cells. *Nature* 2017;552(7685):404–409.

50. Kasakovski D, Xu L, Li Y. T cell senescence and CAR-T cell exhaustion in hematological malignancies. *J. Hematol. Oncol.J Hematol Oncol* 2018;11(1):91.

51. Kang CB, Hong Y, Dhe-Paganon S, Yoon HS. FKBP family proteins: immunophilins with versatile biological functions. *Neurosignals* 2008;16(4):318–325.

52. Milone MC et al. Chimeric Receptors Containing CD137 Signal Transduction Domains Mediate Enhanced Survival of T Cells and Increased Antileukemic Efficacy In Vivo. *Mol. Ther.* 2009;17(8):1453–1464.

53. McPherson M, Yang Y, Hammond PW, Kreider BL. Drug receptor identification from multiple tissues using cellular-derived mRNA display libraries. *Chem. Biol.* 2002;9(6):691–698.

54. Sather BD et al. Efficient modification of CCR5 in primary human hematopoietic cells using a megaTAL nuclease and AAV donor template. *Sci. Transl. Med.* 2015;7(307):307ra156.

Figure 1

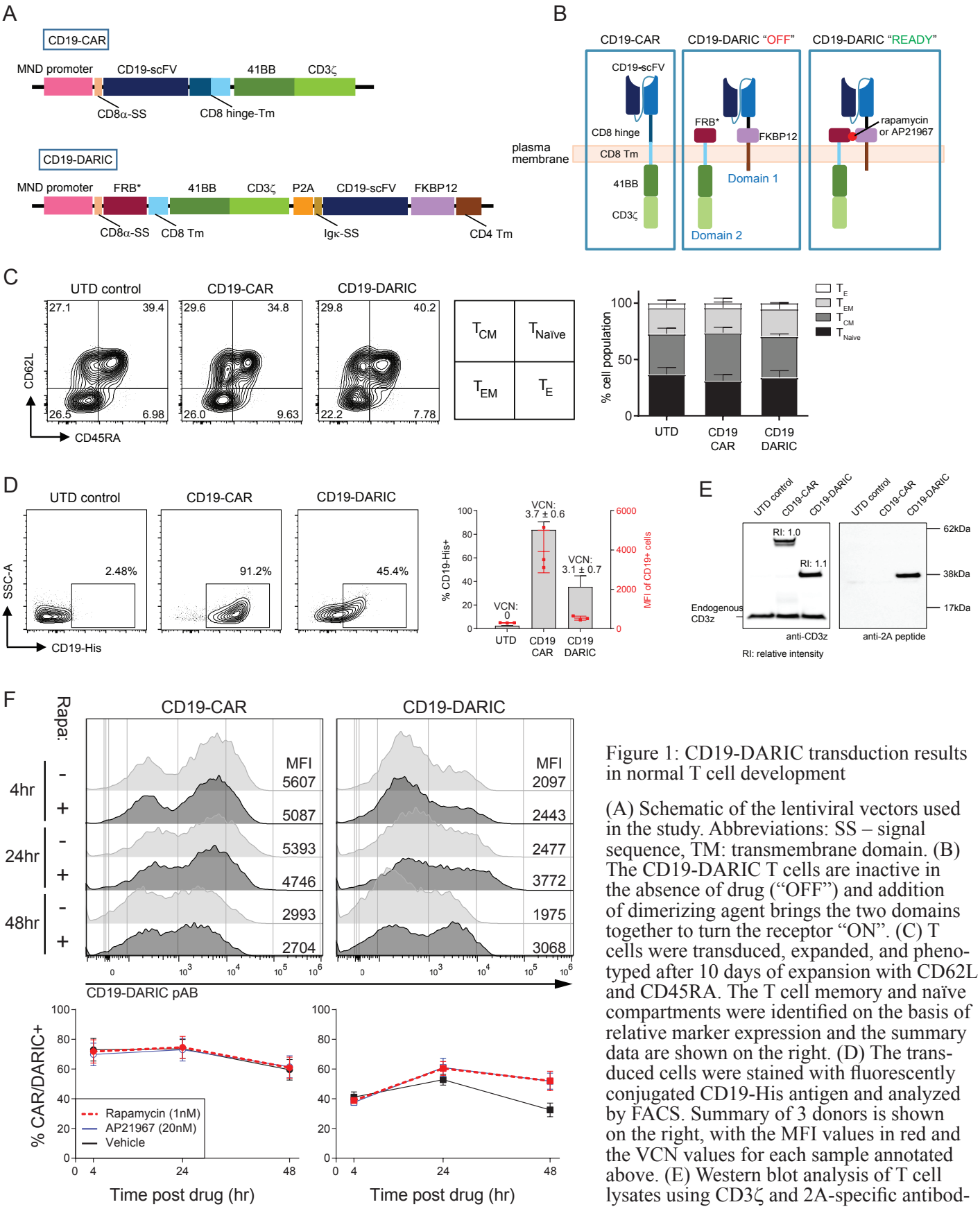

Figure 1: CD19-DARIC transduction results in normal T cell development

(A) Schematic of the lentiviral vectors used in the study. Abbreviations: SS – signal sequence, TM: transmembrane domain. (B) The CD19-DARIC T cells are inactive in the absence of drug ("OFF") and addition of dimerizing agent brings the two domains together to turn the receptor "ON". (C) T cells were transduced, expanded, and phenotyped after 10 days of expansion with CD62L and CD45RA. The T cell memory and naïve compartments were identified on the basis of relative marker expression and the summary data are shown on the right. (D) The transduced cells were stained with fluorescently conjugated CD19-His antigen and analyzed by FACS. Summary of 3 donors is shown on the right, with the MFI values in red and the VCN values for each sample annotated above. (E) Western blot analysis of T cell lysates using CD3ζ and 2A-specific antibodies. Relative intensity was determined using LICOR western blot analysis software. (F) CD19-CAR or CD19-DARIC T cells were cultured for the indicated amount of time in the presence or absence of rapamycin. The expression of the CAR/DARIC construct was analyzed by staining with rabbit polyclonal anti-CD19 complex antibody. The summary of the staining data is shown below. Error bars represent three unique donors. Data are representative of at least 3 separate experiments, with 3 unique donors per experiment.

Figure 2

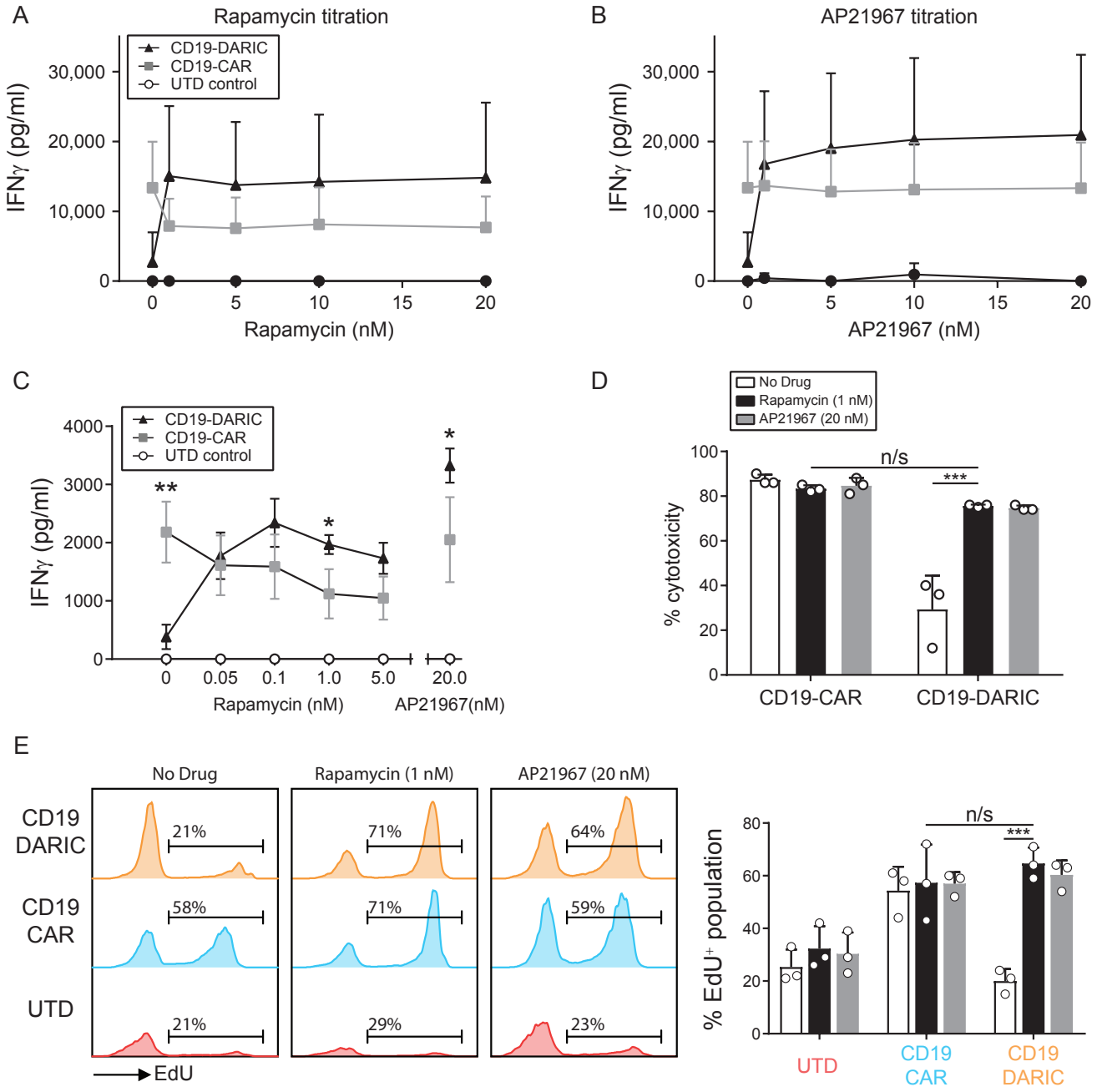

Figure 2: CD19-DARIC T cells are tumor-reactive solely in the presence of a dimerization drug

(A-C) The CD19-CAR and CD19-DARIC T cells were cultured at a 1:1 ratio with fluorescent Nalm6 target cells with or without different concentrations of either rapamycin or AP21967. Supernatant was collected 24hr after culture initiation and cytokine levels were analyzed using IFNγ-specific ELISA (A&B) or iQue QBead assay (C). N=3, * $p<0.05$; ** $p<0.01$; as determined by a two tailed unpaired Student's *t*-test. (D) The % cytotoxicity was determined by analyzing the ratio of fluorescent Nalm6 cells to antigen-naïve K562 cells following a 24hr co-culture with CAR or DARIC T cells. *** $P<0.001$ using one way ANOVA analysis with Dunnett's test for multi-parameter comparison to CD19-DARIC T cells cultured with rapamycin. (E) The T cells were co-cultured with Nalm6 for 72hr in indicated conditions. Modified EdU was added and the cells were cultured for another 24hr prior to analysis of EdU incorporation. The percent of EdU+ cells represents the proportion of cells that underwent DNA synthesis in the prior 24hrs. *** $P<0.001$ using one way ANOVA analysis with Dunnett's test for multi-parameter comparison to CD19-DARIC T cells cultured with rapamycin. n/s: not significant.

Figure 3

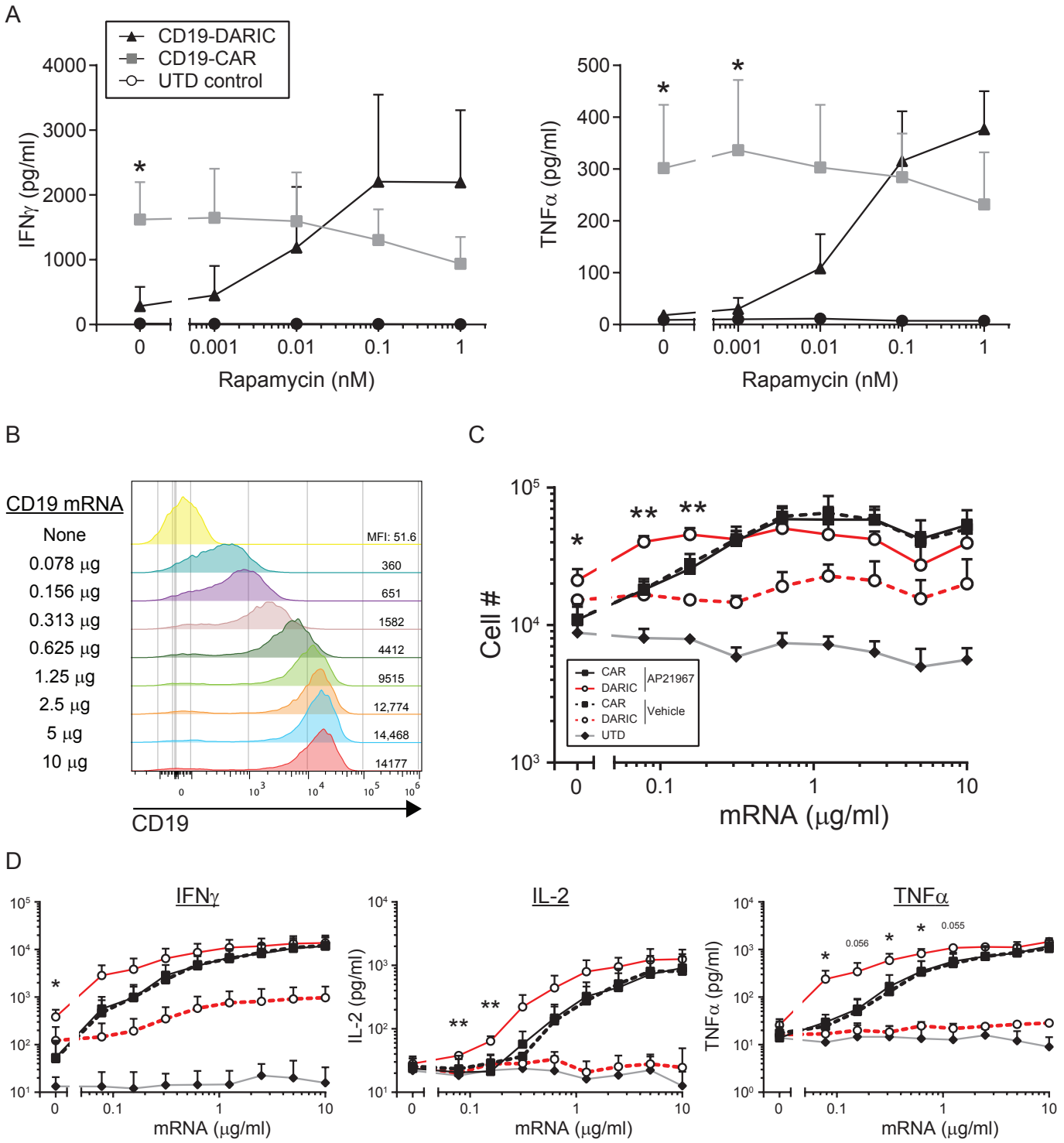

Figure 3: CD19-DARIC T cells are potent even at low rapamycin concentrations and low antigen expression

(A) The CD19-DARIC or CD19-CAR T cells were cultured with Nalm6 cells for 24hr in the presence of different concentrations of rapamycin. Cytokine production was analyzed using iQue QBeads. Error bars represent 3 donors. (B) K562 cells were transfected with *in vitro* transcribed mRNA encoding the CD19 antigen. The transfected cells were cultured for 24 hours and CD19 expression was analyzed by flow cytometry. The amount of CD19 mRNA for each transfection is shown on the left while the CD19 MFI value is listed on the right. (C) The CD19 transfected K562 cells were cultured with CD19-DARIC (red) or CD19-CAR (black) T cells in the presence of 20nM AP21967. After a 24hr incubation period, supernatant was collected for cytokine analysis and cells were cultured for an additional 72hrs (4 days total co-culture). At the conclusion of the co-culture period, the number of T cells in each well was counted. The dashed lines represent samples cultured without AP21967 while straight lines represent samples cultured in the presence of 20nM AP21967. The gray line is shown as an untransduced control. (D). Cytokine production in 24hr supernatants from (C) was analyzed using iQue QBeads. Error bars represent 3 unique donors. * $p<0.05$; ** $p<0.01$; as determined by a two tailed unpaired Student's *t*-test comparing AP21967 treated CD19-DARIC T cells vs. AP21967 CD19-CAR samples.

Figure 4

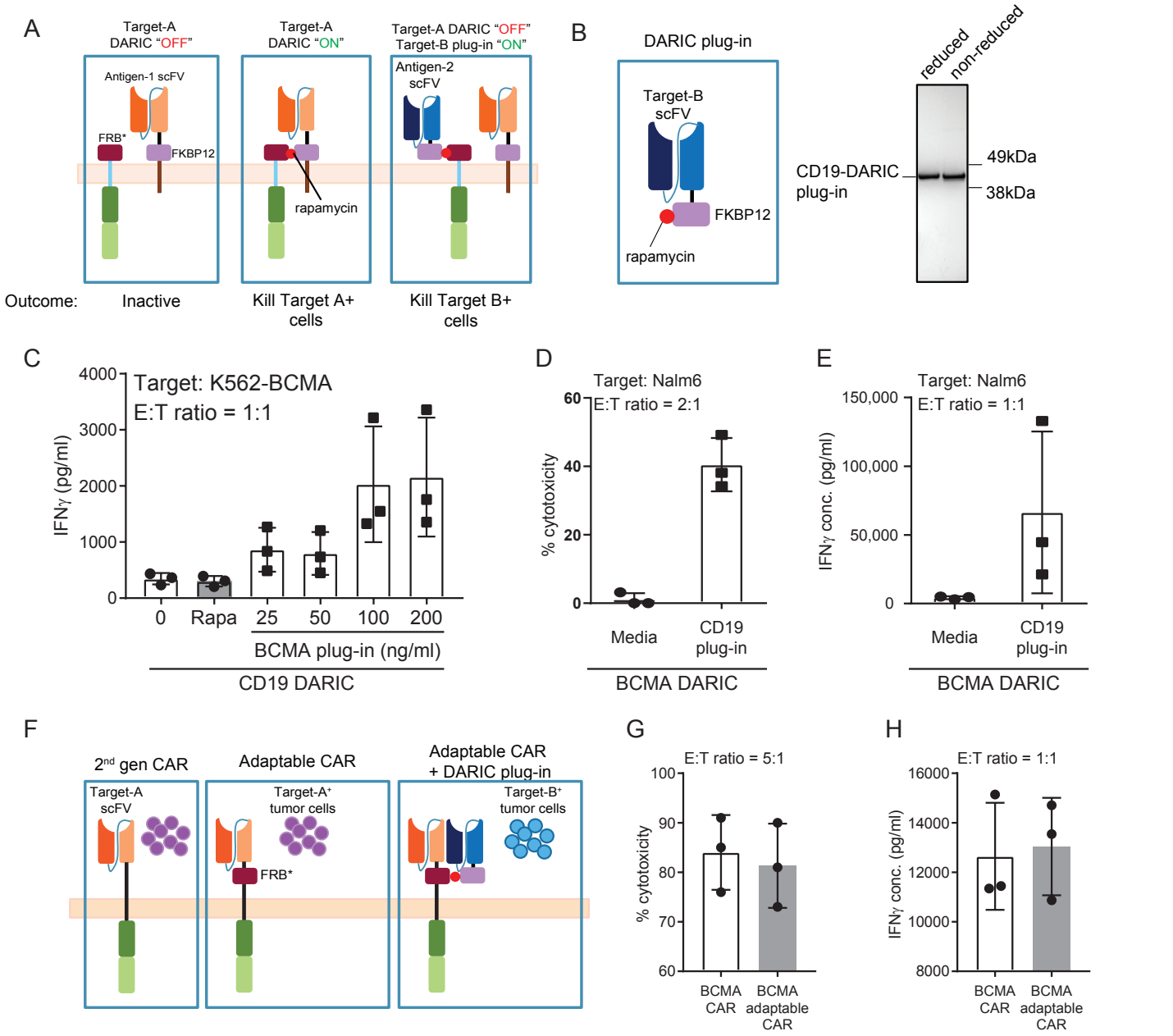

Figure 4: DARIC T cells recognize secondary antigens through the DARIC plug-In system

(A) Schematic of a DARIC signaling architecture in the presence or absence of a DARIC plug-in targeting a 2nd antigen. (B) The recombinant CD19-DARIC plug-In was produced and purified from suspension of 293T cells using a rapamycin-based affinity column. The purified protein was analyzed using coomassie blue staining. (C) Unmodified CD19-DARIC T cells were co-cultured with K562-BCMA cells either alone, in the presence of rapamycin, or in the presence of increasing concentration of rapamycin pre-loaded BCMA plug-in. Cytokine production was analyzed by iQue QBeads. (D) The cytotoxicity and (E) cytokine production of BCMA-DARIC T cells co-cultured with CD19+ Nalm6 cells in the presence or absence of rapamycin pre-loaded CD19 DARIC plug-in. (F) Schematic of adaptable CAR architecture, with an extracellular FRB* domain located next to the scFv able to bind recombinant DARIC plug-in scFv to target a secondary antigen. (G) The cytotoxicity and (H) Interferon-γ cytokine production of BCMA-adaptable CAR following 24hr co-culture with K562-BCMA target cells was analyzed by FACS and QBeads, respectively. (I) The cytotoxicity and (J) cytokine production of control and BCMA-adaptable CAR in the presence of recombinant CD19-DARIC plug-in was analyzed after 24hr co-culture with Nalm6 target cells. Error bars represent 3 different donors.

Figure 5

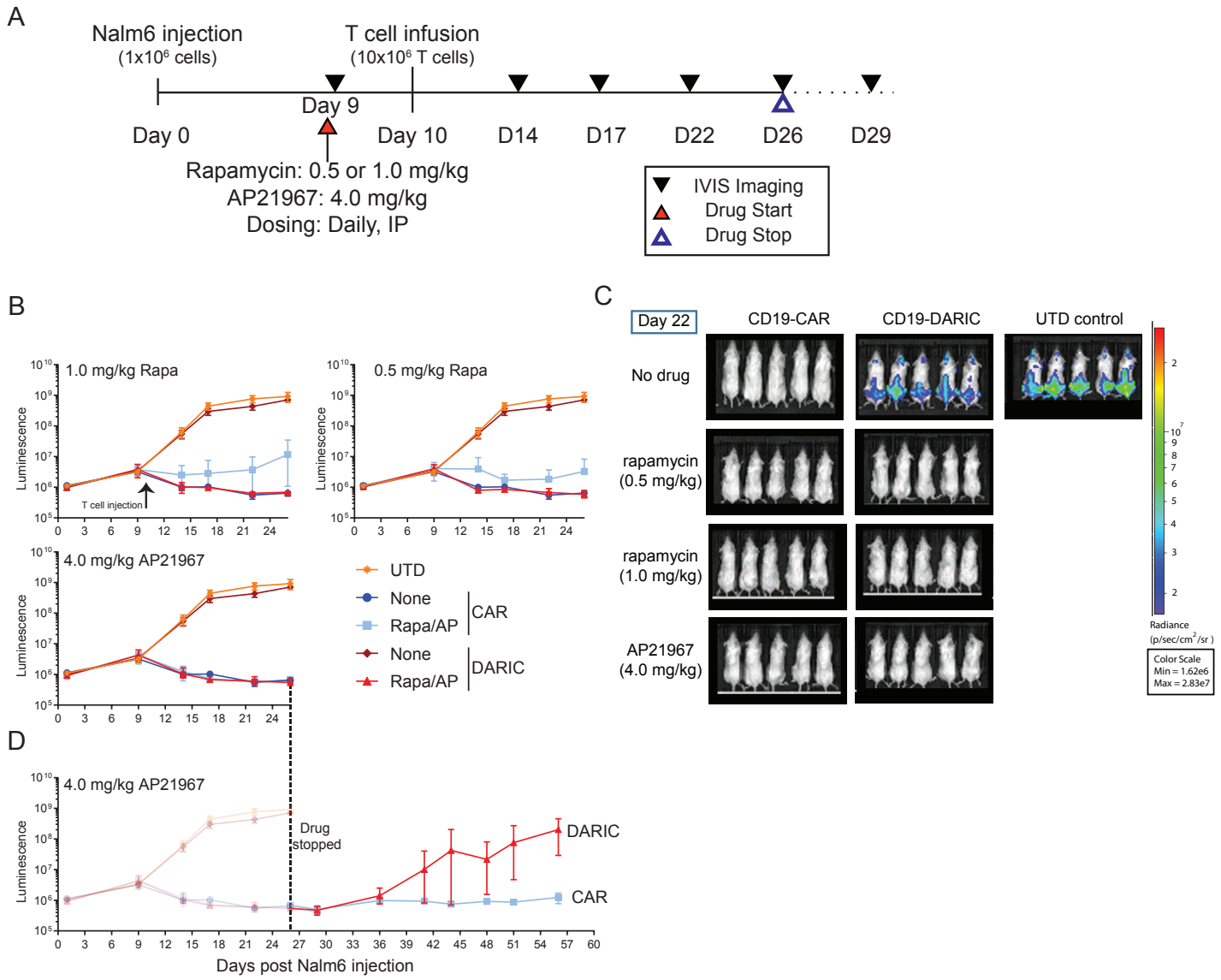

Figure 5: DARIC T cells exhibit drug-mediated tumor control *in vivo*

(A) Outline of the *in vivo* experiment for testing CD19-DARIC T cells. The T cells were infused 11 days following tumor injection while drug dosing started one day prior to T cell injection. (B) Summary bioluminescence data for each drug control group. The UDT and the no drug CAR/DARIC groups are the same for all figures, while the "+ drug" groups (light blue and red) represent the specific drug dose used for the group. Error bars represent 5 mice. (C) Representative bioluminescence imaging at day 22 following tumor injection. (D) Bioluminescence tumor imaging of the AP2167 group followed for additional 20 days after drug dosing was stopped.

Figure 6

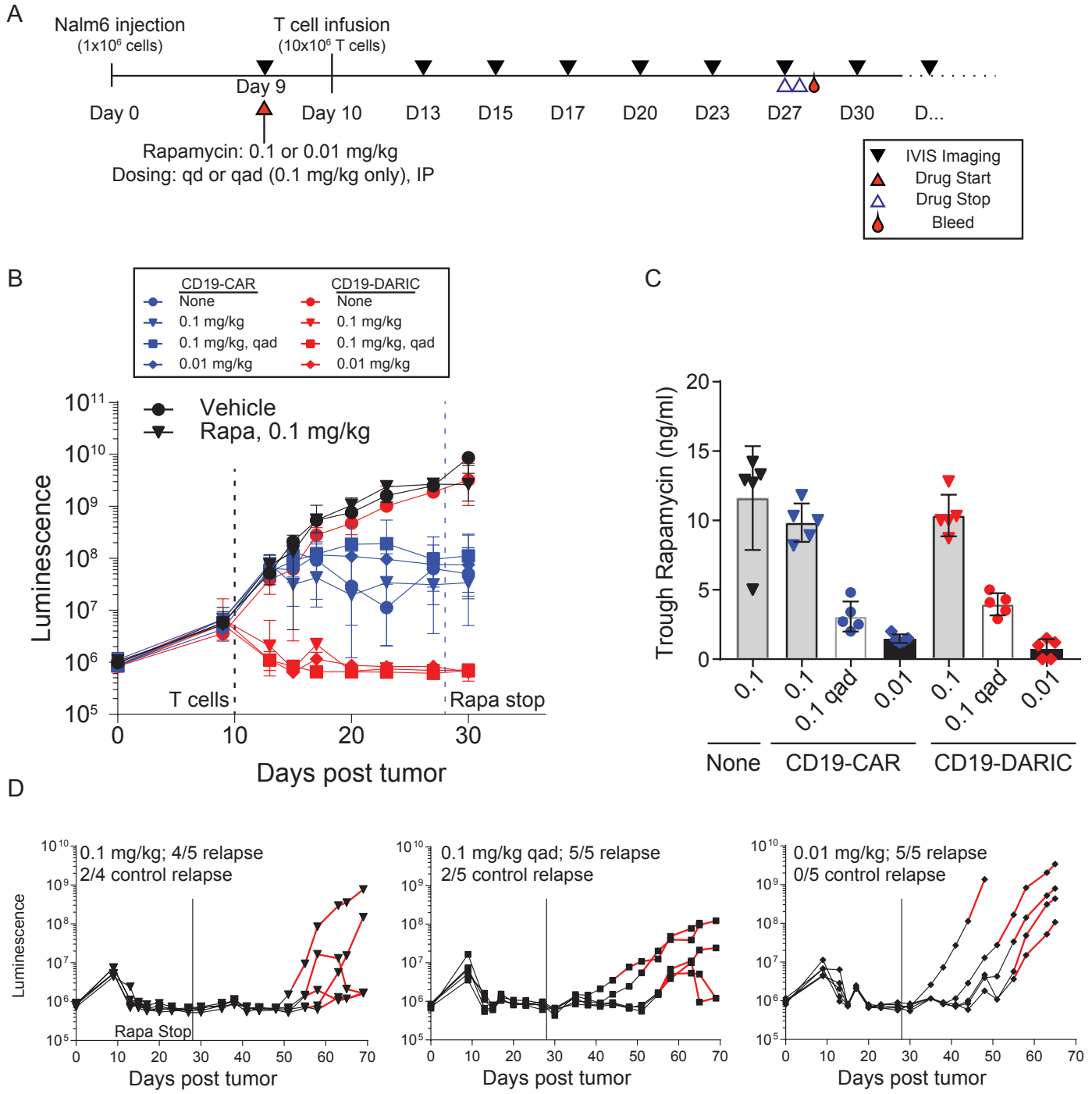

Figure 6: CD19-DARIC T cells control tumor growth *in vivo* with non-immunosuppressive rapamycin dosing

(A) Outline of the *in vivo* experiment for analyzing CD19-DARIC activity at low rapamycin dosing. (B) Summary bioluminescence reading for all the experimental groups. Black and blue dashed lines represent initial T cell injection and cessation of rapamycin dosing, respectively. Error bars represent mean and standard deviation of five animals per group. (C) Trough rapamycin levels in whole blood were analyzed by liquid chromatography-tandem mass spectrometry (LC-MS/MS). Analysis was done at 24hr (0.1 and 0.01) or 48hr (0.1 qad) following last rapamycin injection. (D) The bioluminescence traces for individual animals from each dose group shown in (B) are represented as black lines. The animals were tracked by regular imaging and rapamycin dosing was restarted when tumor regrowth was detected (red lines).